NASA Technical Memorandum 110229

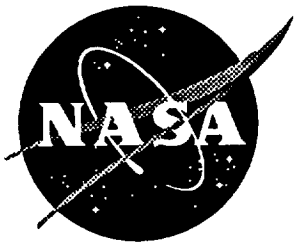

Wing Twist Measurements at the National Transonic Facility

A. W. Burner, R. A. Wahls, and W. K. Goad
Langley Research Center, Hampton, Virginia

February 1996

National Aeronautics and
Space Administration
Langley Research Center
Hampton, Virginia 23681-0001

WING TWIST MEASUREMENTS AT THE NATIONAL TRANSONIC FACILITY

A.W. Burner
R.A. Wahls
W. K. Goad

ABSTRACT

A technique for measuring wing twist currently in use at the National Transonic Facility is described. The technique is based upon a single camera photogrammetric determination of two dimensional coordinates with a fixed (and known) third dimensional coordinate. The wing twist is found from a conformal transformation between wind-on and wind-off 2-D coordinates in the plane of rotation. The advantages and limitations of the technique as well as the rationale for selection of this particular technique are discussed. Examples are presented to illustrate run-to-run and test-to-test repeatability of the technique in air mode. Examples of wing twist in cryogenic nitrogen mode are also presented.

INTRODUCTION

Model deformation may be defined as the change in shape of a model (particularly the wings and control surfaces) under aerodynamic load in a wind tunnel. This change in the design geometry can cause differences between the acquired and expected wind tunnel results if the expected results are based upon rigid body assumptions. Differences can also occur between acquired wind tunnel data and computational predictions based upon rigid body assumptions. These differences can lengthen and degrade the aircraft design process. The measurement of model deformation has thus been of interest for over 20 years and was identified as especially desirable for the National Transonic Facility (NTF) as early as the mid 1970's. More recently, widespread interest in the potential for measuring surface pressure distributions with pressure sensitive paints (PSP) has renewed the importance of model attitude and deformation measurements under aerodynamic loads, because of requirements to ratio wind-off and wind-on images between which the model has moved and changed shape.

The fundamental technique used to measure model deformation continues to be photogrammetry as was the case 20 years ago, but today electronic imagers are used in place of film cameras. The rapid development of relatively low cost electronic imaging, largely driven by the consumer video market, coupled with improvements in low cost computing have enabled the application of video photogrammetric techniques to a number of different types of measurement problems, including model deformation. Video photogrammetric systems are available, but these systems are generally not suitable for incorporation into a wind tunnel data acquisition system because of the user interaction required. In addition, limited view ports, low contrast targets, and limited illumination options all contribute to the requirement for custom measurement systems for many wind tunnels. In some wind tunnel tests (ref. 1) 2-dimensional video imagers have been

replaced with 1-dimensional linear arrays and active infrared sources are used as targets instead of passive rub-on or painted targets. This combination of 1-dimensional arrays and active sources more readily enables automation of the measurement, provided the installation of active targets is acceptable. A good example of this latter type of system is the Optotrak® system made by Northern Digital Inc. of Canada. This system is capable of determining 3-dimensional locations at up to 600 Hz (for a limited number of markers). Well-controlled laboratory static calibration tests at Northern Digital have shown that the rms error in angle of attack (AOA) measurements can approach several arcseconds over a range of 180° (ref. 2). One disadvantage of the Optotrak® system is that infrared light emitting diodes (LED's) must be placed in the model as markers. These markers must then be activated in sequence to provide real time maker discrimination. Another problem with the Optotrak® measurement system is the relatively large size of the image sensors which may make it difficult to adapt for use in some wind tunnels.

NATIONAL TRANSONIC FACILITY MODEL DEFORMATION BACKGROUND

The National Transonic Facility is a fan-driven, closed-circuit, continuous-flow pressurized wind tunnel (ref. 3). The 8.2 x 8.2 x 25-ft long test section has a slotted-wall configuration. The wind tunnel can operate in an elevated temperature mode up to T = 140° F, normally using air, and in a cryogenic mode, using liquid nitrogen as a coolant, to obtain a test temperature range down to about -250° F. Thermal insulation inside the pressure shell minimizes energy consumption. The design total pressure range for the NTF is from 15 psia to 130 psia. The combination of pressure and cold test gas can provide a maximum Reynolds number of 120,000,000 at Mach 1.0, based on a chord length of 9.75 inches. These characteristics afford full-scale Reynolds number testing for a wide range of aircraft. Three types of investigations are possible: Reynolds number effects at constant Mach number and dynamic pressure; model aeroelastic effects at constant Reynolds number and Mach number; and Mach number effects at constant dynamic pressure and Reynolds number. The constraints imposed by operation in a high pressure environment over such a wide range of temperatures have had a significant impact on instrumentation development for the facility. Even though the facility has been operational since August 1984, instrumentation development, improvement, and optimization are still underway.

Since high aerodynamic loads encountered in the NTF can cause model deformations, a requirement for an instrumentation system to measure model geometry at test conditions was identified early. Several techniques were considered for the measurement including a microwave modulated laser technique, moiré contouring (ref. 4), scanning heterodyne interferometry, holographic techniques (ref. 5), and photogrammetric techniques using either film cameras or image dissector cameras. The photogrammetric approach was selected for initial tests at the NTF largely due to earlier successful tunnel tests with film cameras at the NASA Langley Eight Foot Transonic Pressure Tunnel (ref. 6). It was also thought that there would be fewer tunnel implementation problems with photogrammetry than with the other techniques. Two parallel photogrammetric efforts were initiated for

the NTF. ITT was selected to develop the Stereo Electro-Optical Tracking System (SETS) for the NTF (ref. 7). This rather large developmental effort to provide an automated model deformation measurement system for the NTF was based upon image dissector cameras which at the time were state of the art. A second, smaller, in-house effort concentrated on film photogrammetry in order to more rapidly gain initial lab and tunnel experience. However, in just a few years, the image dissector technology became obsolete due to the rapid advancement in solid state image sensors. The decision was then made to abandon the SETS and concentrate on the in-house effort. For initial tests at the NTF film cameras were replaced with high resolution, 875 scan line, video tube cameras because of inaccessibility of cameras which must be housed within the cryogenic, high pressure plenum. Additional distortions introduced by video tube cameras into the photogrammetric measurement were investigated and techniques to correct for these distortions were evaluated (ref. 8). Initial model deformation tests with the tube-based video photogrammetric technique in both air and cryogenic modes were made soon after the NTF became operational (ref. 9).

Solid state video cameras were chosen for subsequent testing at the NTF since tunnel vibration-induced electronic distortion associated with the camera tube construction severely degraded the video data at low temperature and high pressure (ref. 10). In addition, a personal computer (PC) controlled image acquisition system was employed to eliminate the manual measurement of targets associated with the previous tube camera technique. Camera calibration, data reduction procedures, and laboratory tests to establish the uncertainty of this technique (denoted the Video Model Deformation or VMD system) were reported in reference 10 where the accuracy for measuring wing deflection was shown to be about 0.005 inch rms under best case wind-off ambient conditions over a 26.5 inch semi-span test wing. It was also determined that wing twist measurement errors as large as 0.2° might be experienced under best case wind-off conditions, even with suitable least-squares fits to a large number of targets.

In order to improve the accuracy of the VMD system, laboratory studies were conducted on the calibration and characterization of industrial and scientific solid state area array cameras (refs. 11 and 12). These studies indicated that state of the art calibration techniques and cameras, while helpful under ambient wind-off conditions, were not limiting factors for VMD system performance during wind-on test conditions at the NTF. The harsh environmental conditions at the NTF, which can severely degrade imagery, are thought to be the limiting factors since temperature-induced contractions from ambient to cryogenic conditions, coupled with the high refractive index in the test section, can lead to bias errors in the photogrammetric measurement which are much larger than the precision error. Attempts to develop suitable correction techniques to reduce or eliminate these bias errors were unsuccessful. The technique currently used at the NTF to measure wing twist, however, has the potential to partially compensate for some of the bias errors. The rationale for development of this technique follows.

RATIONALE FOR WING TWIST TECHNIQUE

In discussions about model deformation measurement requirements among a number of people involved in aerodynamic testing, the determination of the induced wing twist under aerodynamic load is considered to be the primary concern, with wing deflection (bending) being of secondary importance. Laboratory investigations, simple error analyses, and preliminary wind tunnel tests at the NTF of wind-on and wind-off conditions indicated that flow-induced wing twist measurement uncertainty was larger than desired. Therefore it was decided to investigate ways to increase the resolution of the photogrammetric technique in order to provide acceptable wing twist uncertainties.

The resolution of photogrammetric measurements generally is inversely proportional to the field-of-view. Thus it is possible to increase resolution at the expense of limited field-of-view by using longer focal length lenses to zoom in on the outboard portion of the wing near the tip. However, once this is done the fuselage is no longer in the field of view to serve as a reference in order to remove the sting deflection component from the wing deflection. Thus, without fuselage deflection data, deflection measurements at various semispan locations will contain this sting deflection component as well as the wing bending. If wing bending is desired, calculated values for sting deflection must be used or a second camera will be required to view the fuselage in order to measure sting deflection.

Photogrammetric data reductions are based upon the collinearity equations which relate the 3-D object coordinates to the 2-D image plane coordinates. For high accuracy static measurements the data reduction procedure of choice in photogrammetry is bundle adjustment with self calibration (ref. 13). In this procedure a single camera is moved to a number of locations (usually 8 or more) at which photographs are taken of a large number of high contrast targets, properly illuminated retroreflective disks, distributed throughout the test field. The 3-dimensional coordinates of the targets along with calibration parameters associated with the camera are computed by a nonlinear least-squares adjustment with the 2-dimensional image plane coordinates, initial guesses for the unknowns, and photogrammetric scale as inputs. Generally, however, this method is not suitable for wind tunnel use because of the dynamic nature of tests. In addition, restricted viewing port locations and the inability to utilize widely distributed high contrast targets limit the practicality of multi-camera applications. Even so, the bundle method with self calibration can still be used for pre-test laboratory camera calibrations (ref. 12). For photogrammetric data reductions where bundle adjustment is inappropriate, cameras are calibrated before installation and the locations and pointing angles of the camera are determined by a space resection method. In space resection, the 2-dimensional image plane coordinates of a number of targets in the field of view with known locations are used as input to a nonlinear least-squares solution of the collinearity equations (ref. 13). Three dimensional coordinates are then found by multi-camera triangulation, sometimes referred to as space intersection, or simply intersection.

In multi-camera photogrammetric measurements of wing twist it is often difficult to simultaneously optimize the lighting for two or more cameras given the wind tunnel

lighting restrictions and the difficult task of illuminating targets on a mirror-like wing surface typical for the NTF, at various AOA setpoints. In addition, for multi-camera photogrammetric measurements, computation of centroids from each image for each data point is required along with precise time synchronization in order to match corresponding fields from the cameras. Target identification and matching between the cameras is also required. However, if a single camera photogrammetric technique can be used, which is possible whenever one of the three target coordinates is known, then these problems are lessened considerably. A single camera technique may also be more amenable to automation. The major limitation of a single camera solution is the requirement that one of the coordinates be known. The error in a single camera solution will then depend on how well the third coordinate is known. In case all coordinates are unknown, then more than one camera is required to find a solution.

A single camera photogrammetric solution is possible during pitch sweeps since motion is confined to the pitch plane, at least for wind-off. During wind-off pitch sweeps the Y coordinate in the spanwise direction of each target does not change; only the X coordinate in the flow direction and the Z coordinate in the vertical direction vary with pitch. If the Y coordinates of all targets are known then a single camera solution exists. To reduce the effect of dynamic yaw motion typical at the NTF, which causes Y to vary, 10 video fields are recorded over a one second data recording interval, from which image plane coordinate means are computed. The mean image plane coordinates are a good approximation to the expected image plane coordinates without dynamic yaw, since over small intervals of Y the collinearity object-image equations are very nearly linear even though they are globally nonlinear.

Once X, Z coordinates are computed, the differences in pitch angle on the wing from wind-off conditions to wind-on conditions are determined by means of a conformal two-dimensional transformation of X, Z coordinates at each semispan location. Least-squares computation of the conformal transformation has several desirable properties. The change in pitch angle and the corresponding displacements in X and Z are determined along with estimates of precision for each variable as a byproduct of the least-squares reduction. The conformal transformation also separates the angular and linear motion. For example, transformations on a pure rotation about a displaced center of rotation will yield the angle of rotation only, not the change in Z coordinates due simply to the offset from the center of rotation.

A major optical instrumentation problem at the NTF has been the wide operational temperature range. In addition to operational problems such as window frosting, the large change in temperature can lead to uniform and non-uniform contractions. These tend to introduce photogrammetric measurement bias errors which are very difficult to quantify. Since attempts at using test section wall targets to account for these bias errors had not been fully successful, it was decided to use wind-off polars at each tunnel condition as reference in the wing twist computation. Wind-on wing twist is then computed as the difference in wing pitch angle between wind-off and wind-on conditions. Since the model pitch angle at wind-on and wind-off test points may not be equal, it is necessary to

subtract out the difference as determined by the primary model pitch angle measurement system, to obtain flow-induced wing twist.

Since the wind-on and wind-off data are computed from images at nearly the same temperature and pressure, the effects of these variables are lessened. If the same model pitch angle is used for the wind-on and wind-off images, then the images from each will be at nearly the same image plane location neglecting sting bending. Thus any potential optical and sensor distortion will be comparable and tend to cancel. This error cancellation is only approximated at wind-on test conditions due to sting deflection and wind-on flow structure such as shock waves or boundary layers which can cause refractive index variations.

EXPERIMENTAL PROCEDURE AND DATA REDUCTION

The optical technique used to determine wing twist data presented herein is based upon the recording and analysis of digitized video images. A video signal from a standard RS-170 solid state camera with 752 horizontal by 240 vertical pixels per field is routed to a frame grabber controlled by a 386-33 MHz PC which records ten video fields in one second into the frame grabber memory. Ten fields are recorded in order to reduce the effects of dynamic yaw as discussed later. Only ten fields are presently recorded, instead of the desired 60 fields in one second, in order to reduce data storage time and volume. The contents of the grabber memory are stored on a hard disc with the current point number as file name. Once the hard disc is full, currently 144 data points, the digital images are transferred to an optical disc for archiving. The charge-coupled device (CCD) video camera used for wing twist measurements at the NTF has an adjustable field integration time in order to reduce the effects of dynamics on image recording. An 11.5 to 69 mm focal length remote zoom lens is currently used for imaging. Considerations when calibrating zoom lenses for wind tunnel use are discussed in reference 14.

The CCD camera is mounted in a protective housing in the test section sidewall. The camera looks over the fuselage at one of the wings of the model (fig. 1). The camera is rotated 90° so that the horizontal X axis is vertical on the image plane in order to provide additional viewing flexibility. In addition, the 90° rotation more nearly matches the number of pixels vertically and horizontally across a target image since perspective causes the images to be longer in the X (streamwise) direction. The protective housing is equipped with insulation and sheath heaters to maintain camera temperature. The housing is pressure rated to greater than 9 atm. In order to prevent frost, air heated by an inline heater flows to a purge ring with a number of holes to direct the heated air over the inside surface of the one inch thick fused silica window viewport. A purge air vent to atmosphere maintains the camera housing pressure at approximately 1 atm.

Circular targets, with an approximate diameter of 5 mm, are applied to the wing surface (fig. 2) with a Sharpie® marking pen. it should be pointed out that such targets have not been acceptable for all test conditions as discussed later. A template is used to place targets in several rows in the streamwise direction. For the data reported here the target

rows were located at normalized semispan locations equal to 0.635, 0.778, and 0.922. Initial X and Y coordinates of the targets are determined from pressure tap and other reference locations on the wing. The Z coordinates are estimated from cross-sectional drawings of the wing.

Data recording is programmed with a script file for automatic acquisition upon trigger as each data point is taken. The use of script files to automatically configure and control the frame grabber menu driven program was convenient for initial developments. The initial data reduction code was written in QuickBASIC 4.5. In order to reduce data acquisition and reduction time, trial versions of code have been written in the C programming language. In these versions, C language functions for the frame grabber are used to control and configure the data recording as well to access frame grabber video memory so that centroids can be computed without first saving the digital images as DOS files. Tests using the trial code on high-contrast targets during both wind-off and wind-on tests at the NASA Langley Transonic Dynamics Tunnel during several recent semispan tests were encouraging.

The initial pre-test calibration procedure for the video optical technique determines those camera parameters necessary for conversion from pixels to corrected image plane coordinates. Techniques for determining these parameters are discussed in references 11 through 14. The need for extensive camera calibration is lessened somewhat by on-line calibration using the model pitch angle for wind-off reference at the tunnel total temperature and pressure test conditions.

The pointing angles and location of the camera in the tunnel coordinate system are determined at the start of the test by photogrammetric resection during a wind-off reference run. A known set of targets for resection are established by merging a range of wind-off points into a single reference target field based on knowledge of the center of rotation and rotation angle. The final calibration step requires a wind-off pitch sweep at run temperature and pressure over the range of angles expected during the wind-on testing.

Image plane coordinates are determined by gray level center-of-mass calculation after inverting the gray scale and subtracting the background plus a few additional gray scales The background is found from the maximum gray scale on the border of a window of pixels which is slightly larger than the target images (ref. 11). The mean pixel coordinates from the ten recorded fields are then transformed and corrected (including correction for the photogrammetric principal point x_p, y_p) to give units of length. The X and Z coordinates are determined from a single camera solution of the following collinearity equations

$$x = -c\frac{[m_{11}(X-X_c)+m_{12}(Y-Y_c)+m_{13}(Z-Z_c)]}{[m_{31}(X-X_c)+m_{32}(Y-Y_c)+m_{33}(Z-Z_c)]}$$

$$y = -c\frac{[m_{21}(X-X_c)+m_{22}(Y-Y_c)+m_{23}(Z-Z_c)]}{[m_{31}(X-X_c)+m_{32}(Y-Y_c)+m_{33}(Z-Z_c)]} \quad (1)$$

where x and y are the corrected image plane coordinates, c is the principal distance (or camera constant) which will be slightly larger than the focal length, X, Y, and Z are the object space coordinates of the target, X_c, Y_c, and Z_c are the coordinates of the perspective center, and the m terms are elements of the following rotation matrix

$$\begin{aligned}
m_{11} &= \cos\phi\cos\kappa \\
m_{12} &= \sin\omega\sin\phi\cos\kappa + \cos\omega\sin\kappa \\
m_{13} &= -\cos\omega\sin\phi\cos\kappa + \sin\omega\sin\kappa \\
m_{21} &= \cos\phi\sin\kappa \\
m_{22} &= -\sin\omega\sin\phi\sin\kappa + \cos\omega\cos\kappa \\
m_{23} &= \cos\omega\sin\phi\sin\kappa + \sin\omega\cos\kappa \\
m_{31} &= \sin\phi \\
m_{32} &= -\sin\omega\cos\phi \\
m_{33} &= \cos\omega\cos\phi
\end{aligned} \quad (2)$$

The pointing angles of the camera, ω, ϕ, and κ, which rotate about the X, Y, and Z axes respectively, are defined as positive if they are counterclockwise when viewed from the positive end of their axes. The X and Z coordinates determined from the collinearity equations (1) for a single camera solution are given below

$$X = X_c + (Y - Y_c)(a_2 a_6 - a_5 a_3)/(a_4 a_3 - a_1 a_6) \quad (3)$$

$$Z = Z_c - (X - X_c)\, a_1/a_3 - (Y - Y_c)\, a_2/a_3 \quad (4)$$

where

$$\begin{aligned}
a_1 &= x m_{31} + c m_{11} \\
a_2 &= x m_{32} + c m_{12} \\
a_3 &= x m_{33} + c m_{13} \\
a_4 &= y m_{31} + c m_{21} \\
a_5 &= y m_{32} + c m_{22} \\
a_6 &= y m_{33} + c m_{23}
\end{aligned} \quad (5)$$

Expression (4) above is suitable for use at the NTF where the camera is rotated 90° so that the horizontal X axis is vertical on the image plane. When the camera is not rotated, the a_3 term is nearly zero so that a_1, a_2, and a_3 in expression (4) should be replaced with a_4, a_5, and a_6 respectively.

The wind-on data at each semispan location is then matched with a wind-off point with similar model pitch angle to determine angle and displacement and corresponding standard deviations, using the following least squares conformal transformation

$$X' = X \cos \theta - Z \sin \theta + T_x$$
$$Z' = X \sin \theta + Z \cos \theta + T_z \qquad (6)$$

where T_x and T_z are the translation terms in the X and Z directions and X' and Z' are the coordinates of the wind-off reference point. If a nonlinear least-squares method is used for the conformal transformation, at least two targets are required for one degree of freedom. If a linear least-squares technique is used to solve for a and b rather than the angle directly, where $a = \cos \theta$ and $b = \sin \theta$, a minimum of three targets is needed for one degree of freedom since scale is implicit in the a and b terms without the constraint that a^2 plus b^2 be equal to one. In the linear least-squares solution, the standard deviation of the rotation angle is not computed directly, but is instead computed from the standard deviations of the a and b coefficients. However, given three or more targets, nearly identical results have been obtained with both nonlinear and linear-least squares conformal transformations.

The model pitch angle, measured with an onboard accelerometer package, of the wind-off reference point, α_{off}, is added to the angle θ found above in (6) to yield the streamwise wing angle at a particular semispan location. The wing twist due to aerodynamic load, θ_{twist}, is then found by subtracting the model pitch angle of the wind-on point, α_{on}, or

$$\theta_{twist} = \theta + \alpha_{off} - \alpha_{on} \qquad (7)$$

WING TWIST EXAMPLES AND ERROR CONSIDERATIONS

Examples of repeated measurements of wing twist are presented below. The total uncertainty is expressed as the sum of systematic, or bias error, and precision, or repeatability error. Bias errors are generally very difficult to determine under flow conditions, whereas repeatability can be computed. In addition to laboratory and wind tunnel wind-off determinations of error, run-to-run and test-to-test repeatabilities can be used to gauge the adequacy of wing twist measurements with flow.

The uncertainty requirements for measurement of wing twist caused by aerodynamic loads are unresolved. It has been suggested that the desired uncertainty for wing twist which corresponds to an uncertainty of 0.01° for the model pitch angle is of the order of 0.05°, not 0.01°. In other words, an uncertainty of the order of 0.05° in wing twist is thought to have about the same magnitude effect on drag measurements as 0.01° uncertainty in model pitch angle.

Wing twist measurement error can occur due to errors in the camera position and pointing angles which are used in equations (2) through (5) to determine the X and Z coordinates.

Pre-test calibration errors can also contribute to wing twist error if, for instance, incorrect lens distortion or frame grabber affinity corrections are used. Also note from equation (7) that errors in wind-off reference angle, α_{off}, and wind-on angle, α_{on}, will contribute to the error in the wing twist angle, θ_{twist}, although generally the expected error in α_{off} is much smaller than the error in α_{on}.

The Y coordinate, assumed to be known for the single camera solution, is constant and well-behaved for ambient wind-off pitch sweeps. This is verified by independent measurements in the test section as well as by the single camera technique, which typically has an rms error of 0.03° or less when compared to the onboard inertial angle sensor under wind-off ambient conditions. However, Y is not constant during wind-on conditions due to model yaw dynamics and wing bending. Lateral model motion is as large as ± 3 mm based on video images from a test section ceiling camera. This variation in Y contributes to the precision error. Recording 10 images over one second to determine mean image coordinates reduces this error in Y by averaging. Note also that any remaining error in Y will be nearly the same for all wing targets. This is verified by plots of the variation in the pixel coordinates of the targets as a function of time which show that the variations are typically equal to within a fraction of a pixel even for total excursions of several pixels. Thus as long as the image locations are not too far separated, the errors in X and Z will also be similar and will tend to partially cancel out in the conformal transformation (6) used to determine angle θ.

Wing bending causes the Y coordinate of wing targets to decrease which causes a bias error in the computation of X and Z. Assuming a 2nd order bending dependence, a wing tip deflection of 20 mm, and semispan equal to 580 mm, the change in Y value due to wing bending would be approximately 0.5 mm for targets at the tip. The shift in Y for targets inboard of the tip would decrease rapidly. Targets at the same semispan station will experience only slight differences in both bending and shifts in Y value. Note that it is this small difference in bending between fore and aft targets which produces wing twist for swept wings under load. For instance, fore and aft targets in the streamwise direction at the wing tip of the previous example would experience a wing twist of almost -2° for a 30° swept-back wing. For two targets at the tip separated by 50 mm the difference in bending would be 1.7 mm out of a total bending of 20 mm with a corresponding difference in the shift of the Y value for the two targets of 0.06 mm. A shift in Y value of 0.06 mm will cause a difference in image scale between the fore and aft targets of only 1.00003 for typical object distances at the NTF (~1.8 m). For the geometry used at the NTF the error in angle caused by this small difference in scale will be negligible compared to other error sources.

Wind-off: Data illustrating possible error for the video wing twist technique without flow, are presented in Table 1. Two wind-off runs taken on adjacent days were used to compute apparent wing twist, which ideally should be zero without flow. The temperature for both runs was nearly the same (~105° F), but the pressure for these two runs differed considerably (20 and 94 psia). The AOA range for both runs was from 0° to 22°. The mean error and standard deviation of the error for the 13 data points are

presented for the three normalized semispan stations ($Y/b/2$) equal to 0.635, 0.778, and 0.922. Only three wing targets were used at $Y/b/2 = 0.922$, whereas four wing targets were used at 0.778 and 0.635. The wing twist error for $Y/b/2 = 0.922$ is presented in figure 3. The "error bars" in the figure represent the computed standard deviation from the conformal least squares adjustment for each data point and should not be confused with the standard deviations denoted by σ presented in Table 1. Note that normally the wind-off run used as reference in determining wing twist would be taken within an hour at the same total temperature and pressure as the wind-on run. Thus the data in Table 1 may be taken to be a conservative estimate of possible wind-off error at non-cryogenic conditions.

$Y/b/2$	0.635	0.778	0.922
mean	-0.001	-0.018	-0.019
σ	0.018	0.026	0.016

Table 1. Error in degrees when measuring wing twist without flow using a wind-off run from the previous day as reference.

Run-to-run repeatability: The repeatabilities of the video wing twist technique from run-to-run on the same day of a low aspect-ratio research model during air runs are presented for Mach number, M, of 0.3 and dynamic pressure, Q, of 153 psf in Table 2 and $M = 0.9$ and $Q = 965$ psf in Table 3. The results for 4 runs with 30 data points per run are shown in Table 2. Results for 4 runs with 23 data points per run are shown in Table 3. Wing twist, θ_{twist}, was computed at normalized semispan stations 0.635, 0.778, and 0.922 with equation (7). The mean and maximum of the computed sample standard deviation of each repeat set of four data points are denoted as σ_{mean} and σ_{max} in the tables. The arcsector AOA sensor (*ARCSEC*) is much less affected by test dynamics than the onboard accelerometer so that σ_{mean} for the *ARCSEC* variable may be taken as an indicator of model pitch angle variability for repeat points. These two tables show that the mean standard deviation in θ_{twist} for repeat points was less that 0.02° in air mode. In general the standard deviation of the wing twist, θ_{twist}, is less than the standard deviation of the angle, θ, since any real variations in angle-of-attack settings between repeat points present in θ are subtracted out when θ_{twist} is computed. However, note that any error and variability in the onboard angle of attack for α_{on} or α_{off} will be added to the θ_{twist} value. Plots of the repeatability versus α_{on} are presented in figures 4 and 5 for $Y/b/2 = 0.922$ which show worse repeatability at higher α_{on}, especially at the higher Mach number and Q. Data for the other two semispan stations behaved similarly. The corresponding wing twist plots are presented in figures 6 and 7 where the error bars (which are plotted if greater than the symbol size) represent plus and minus one standard deviation of the four repeats at each α_{on}.

	Y/b/2 =	0.635		0.778		0.922	
	$\Delta ARCSEC$	$\Delta\alpha_{on}$	$\Delta\theta_{twist}$	$\Delta\theta$	$\Delta\theta_{twist}$	$\Delta\theta$	$\Delta\theta_{twist}$	$\Delta\theta$
σ_{mean}	0.010	0.011	0.008	0.009	0.007	0.012	0.006	0.018
σ_{max}	0.015	0.019	0.019	0.018	0.024	0.029	0.017	0.018

Table 2. Run-to-run repeatability in degrees for four repeat air runs at $M = 0.3$ and $Q =$ 153 psf.

	Y/b/2 =	0.635		0.778		0.922	
	$\Delta ARCSEC$	$\Delta\alpha_{on}$	$\Delta\theta_{twist}$	$\Delta\theta$	$\Delta\theta_{twist}$	$\Delta\theta$	$\Delta\theta_{twist}$	$\Delta\theta$
σ_{mean}	0.006	0.011	0.016	0.016	0.013	0.015	0.014	0.016
σ_{max}	0.012	0.015	0.029	0.032	0.025	0.033	0.037	0.051

Table 3. Run-to-run repeatability in degrees for four repeat air runs at $M = 0.9$ and $Q =$ 965 psf.

Upright and inverted runs: Inverted model runs are conducted to determine flow angularity by comparison to upright runs. For two inverted air runs targets were placed on the underside of the opposite wing normally viewed to determine wing twist. When the model was inverted 180° these targets were then in the field of view of the wing twist camera so that wing twist measurements could be made to compare to upright runs at the same conditions to provide an error check with flow. A wind-off inverted run was used as reference to compute the wing twist, making proper allowance for change in angle signs due to the inversion. Data from runs made at $M = 0.3$ and $Q = 153$ psf are presented in Table 4 and data from runs made at $M = 0.9$ and $Q = 965$ psf are presented in Table 5. Since the model pitch angle at which the data were taken did not necessarily coincide between upright and inverted, linear interpolation (extrapolation for end points) was used to determine twist values at the midpoint of the pitch angle between nearest data points. Nine data points over a model pitch range of -3° to 5° were used in the computations for Tables 4 and 5.

Y/b/2	0.635	0.778	0.922
mean	-0.045	-0.018	-0.013
σ	0.035	0.023	0.032

Table 4. Mean and standard deviation, σ, in degrees for the differences between upright and inverted air runs at $M = 0.3$ and $Q = 153$ psf at various semispan locations, $Y/b/2$.

Y/b/2	0.635	0.778	0.922
mean	-0.010	-0.002	0.038
σ	0.030	0.051	0.042

Table 5. Mean and standard deviation, σ, in degrees for the differences between upright and inverted air runs at $M = 0.9$ and $Q = 965$ psf at various semispan locations, $Y/b/2$.

Test-to-test repeatability: Comparisons of repeat runs from two tests separated by over five months are presented in Table 6. Linear interpolation to account for differences in model pitch angle setpoint between the tests was used as described above. The mean and standard deviation, σ, of the differences are presented as a function of semispan location, Mach number, and dynamic pressure. The number of data points used for these comparisons varied from 18 to 26. Wing twist data for these runs at a semispan location of 0.922 are presented in figures 8 through 11. Data from the two tests are represented by different symbols. As an additional example of wing twist, a plot comparing air runs made at different dynamic pressures is presented in figure 12 for $Y/b/2 = 0.922$. The Mach number and total pressure were varied to give the desired dynamic pressure. The error bars represent plus and minus one standard deviation as computed from the least squares conformal transformation (6).

Y/b/2 =		0.635		0.778		0.922	
M	*Q*	*mean*	σ	*mean*	σ	*mean*	σ
0.3	154	-0.012	0.022	-0.013	0.030	-0.006	0.027
0.6	534	-0.004	0.059	0.013	0.071	0.011	0.049
0.3	805	0.022	0.093	0.017	0.109	0.026	0.087
0.9	967	0.001	0.027	-0.016	0.026	-0.005	0.047

Table 6. Test-to-test repeatability in degrees during air mode. Units for dynamic pressure Q are psf.

Wing twist measurements at cryogenic conditions have been limited by frosting on the inside surface of the window of the camera protective housing. In the past, the amount of window frosting gradually increased as the tunnel remained cold for long periods of time causing a degradation in video imagery. Additional wing twist data are needed before the run-to-run and test-to-test repeatability under cryogenic conditions can be evaluated. Preliminary wing twist data for two runs under cryogenic conditions are presented in figures 13 and 14. The data are for nitrogen runs at -152° F and -250° F at a semispan location of 0.922. For figure 13 the Mach number was 0.6 and the dynamic pressure was 2670 psf. For figure 14 the Mach number was 0.9 and the dynamic pressure was 1795 psf. The error bars in figures 13 through 14 also represent the standard deviation computed in the least squares conformal transformation (6). Recent improvements during a facility upgrade are expected to improve viewing conditions and flexibility under cryogenic operation and should increase the quality of video data at low temperatures.

FUTURE WORK

Future efforts are expected to include a detailed uncertainty analysis, comparisons between predicted and measured wing twist, and the development of a measurement system for on-line data recording and reduction to provide a nearly automated system. A frame grabber board with dual TMS320C40 digital signal processors is expected to enable data reduction nearly simultaneous to image capture. In addition, innovations are sought

to obtain high contrast, durable wing targets which do not exceed the surface finish requirements at the NTF. The surface finish of models at the NTF can approach 10 microinches, resulting in a "mirror like" surface. Thus images of the wing surface may also contain additional artifacts produced by reflections of a wall or ceiling. In order to successfully automate the wing twist measurement at the NTF high contrast targets are needed which do not exceed the surface finish requirements. These targets should be flat-white solid-filled circles on a flat-black background or the opposite contrast. The currently applied Sharpie® marking pen black targets are neither high contrast nor durable. In addition,some customers of the facility would prefer not to apply the targets due to uncertainty about the effects of the targets on aerodynamic performance; however, results to date do not indicate a measurable adverse effect. Targets applied by a chemical etching technique would be durable, but of low contrast. Gun bluing could also produce durable targets on at least some of the materials used for models at the NTF, but would still produce low contrast targets and have the additional problem of being a "controlled rusting process". Ideas for a suitable target application method at the NTF are solicited.

SUMMARY

The history of the development of a model deformation measurement capability for the National Transonic Facility has been presented. The rationale for the current single camera photogrammetric technique with emphasis on the measurement of wing twist has been presented. The experimental procedure and equations for data reduction have been given. Examples of the measurement of wing twist along with error considerations were given. It has been speculated that the uncertainty for wing twist equivalent to 0.01° model pitch angle may be of the order of 0.05°. The wind-off non-cryogenic 1-sigma error in the measurement technique was shown to be less than 0.03°. Run-to-run repeatabilities in air mode at Mach numbers up to 0.9 and dynamic pressures up to 965 psf were shown to be better than 0.02°. Upright and inverted runs agreed to within 0.05°. Test-to-test repeatabilities of better than 0.03° were also noted. Wing twist measurement examples were presented at tunnel total temperatures of -152° F and -250° F. Future efforts include the use of frame grabbers with onboad digital signal processors and the development of high contrast targets suitable for cryogenic operation which do not exceed the surface finish requirements necessary at the NTF. These efforts should aid in the automation of the measurement.

REFERENCES

1. Smith, D. G. and Crowder, J. P.: The Northern Digital OPTOTRAK® for Wind-On Measurement of Model Deflections. Presented at the 71st Meeting of the Supersonic Tunnel Association, Burbank, CA, April 3-4, 1989.

2. Sherk, T. and Crouch, D. G.: Using the OPTOTRAK®/2010 System for Angle of Attack Measurement. Available from Northern Digital Inc. 403 Albert St., Waterloo, Canada, N2l3V2.

3. Fuller, D. E. and Williams, M. S.: Testing Experience with the National Transonic Facility. AIAA 86-0748-cp. AIAA 14th Aerodynamic Testing Conference West Palm Beach, FL, March 5-7, 1986.

4. Harding, K. and Harris, J.: Evaluation of Moire technique for Wind Tunnel Metrology. UDR-TR-81-111, U. of Dayton Research Institute, Dayton, OH, Oct 1981.

5. Hildebrand, B. P. and Doty, J. L: A Study of Model Deformation Measurement Techniques Applicable Within the National Transonic Facility. NASA CR-165853, Feb. 1982.

6. Brooks, J. D. and Beamish, J. K.: Measurement of Model Aeroelastic Deformations in the Wind Tunnel at Transonic Speeds Using Stereophotogrammetry. NASA TP 1010, Oct. 1977.

7. Hertel, R. J.: Stereo-Electro-Otical Tracker System for the Measurement of Model Deformation at the National Transonic Facility. NASA CR-159146, Oct 1979.

8. Burner, A. W., Snow, W. L., and Goad, W. K.: Close-Range Photogrammetry with Video Cameras. presented at Annual meeting of ASPRS, Washington, Mar. 1985; published in proceedings pp. 62-77.

9. Burner, A. W., Snow, W. L., and Goad, W. K.: Model Deformation Measurements at a Cryogenic Wind Tunnel Using Photogrammetry. 31st ISA Symposium, San Diego, CA, May 1985; published in Instrumentation in the Aerospace Industry - vol 31 ISA pp. 615-622.

10. Burner, A. W., Snow, W. L., Goad, W. K., and Childers, B. A.: A Digital Video Model Deformation System. presented at 12th ICIASF, Williamsburg, VA, June 1987; published in ICIASF '87 RECORD, IEEE, pp. 210-220.

11. Burner, A. W., Snow, W. L., Shortis, M. R., and Goad, W. K.: Laboratory Calibration and Characterization of Video Cameras. presented at ISPRS Symposium: Close-Range Photogrammetry Meets Machine Vision, Zurich, Switzerland, Sept. 1990; published in SPIE Proceedings 1395 pp. 664-671.

12. Shortis, M. R., Burner, A. W., Snow, W. L., Goad, W. K.: Calibration tests of industrial and scientific CCD cameras. Invited paper presented at First Australian Photogrammetry Conference, Sydney, Nov. 7-9, Paper 6, 11 pages, 1991.

13. Karara, H. M., ed.: Non-Topographic Photogrammetry. American Society for Photogrammetry and Remote Sensing, 2nd edition, 1989.

14. Burner, A. W.: Zoom Lens Calibration for Wind Tunnel Measurements. SPIE Proceedings Vol. 2598, pp.19 - 33, Videometrics IV, Philadelphia, PA, Oct. 22-26, 1995.

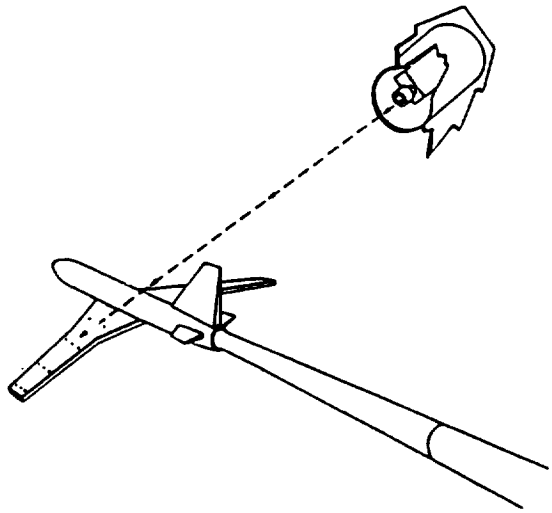

Figure 1. Wing twist camera location at the NTF.

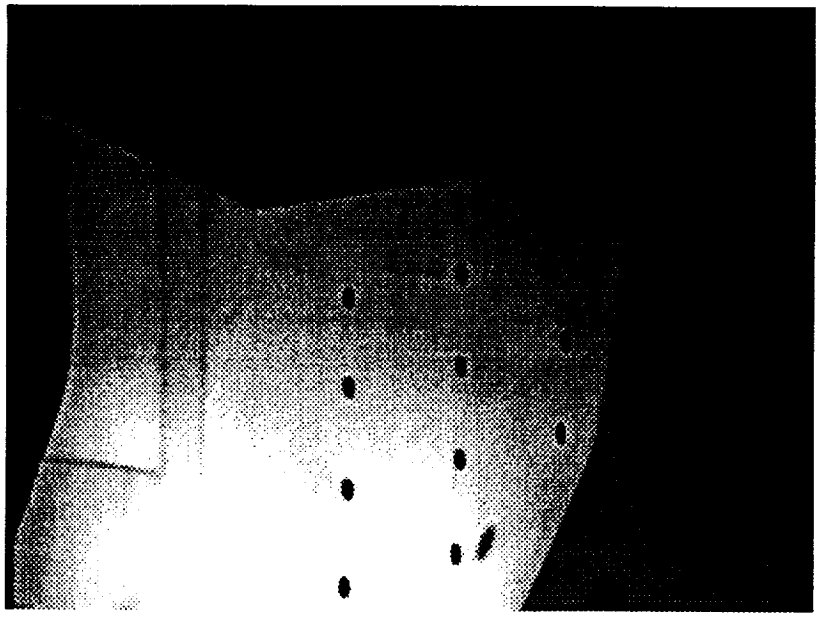

Figure 2. Wing twist camera view. Flow axis is vertical.

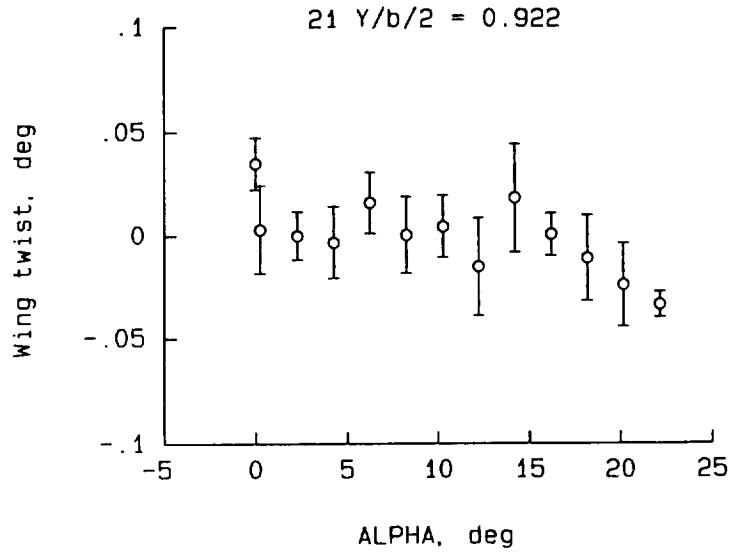

Figure 3. Error in measuring wing twist without flow using a wind-off run from the previous day as reference. The "error bars" in the figure represent the computed standard deviation from the conformal least squares adjustment for each data point.

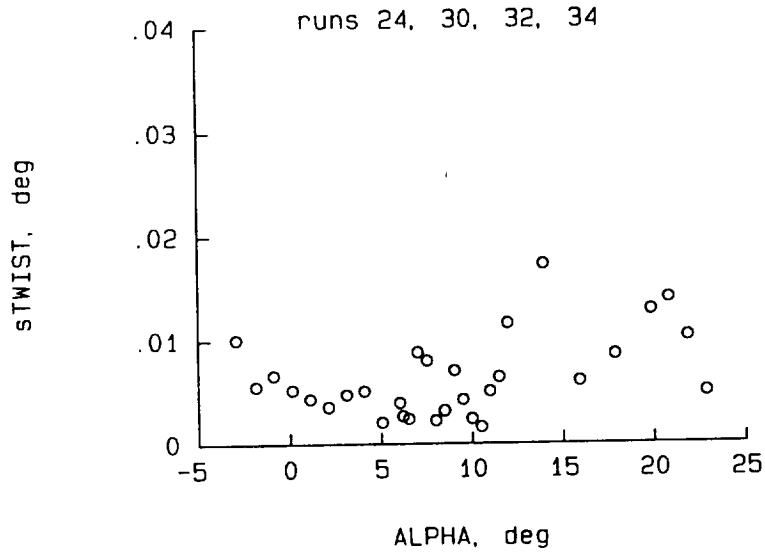

Figure 4. One sigma repeatability corresponding to Table 2 for air runs at Mach = 0.3 and dynamic pressure = 153 psf. Y/b/2 = 0.922.

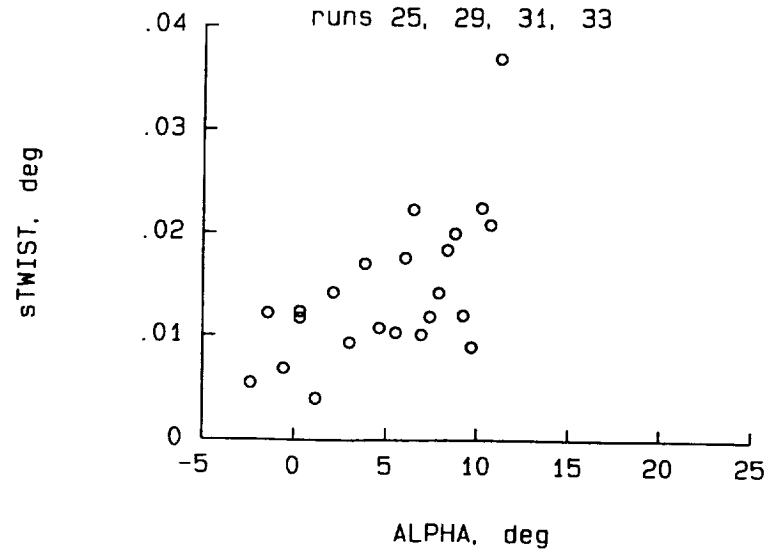

Figure 5. One sigma repeatability corresponding to Table 3 for air runs at Mach = 0.9 and dynamic pressure = 965 psf. Y/b/2 = 0.922.

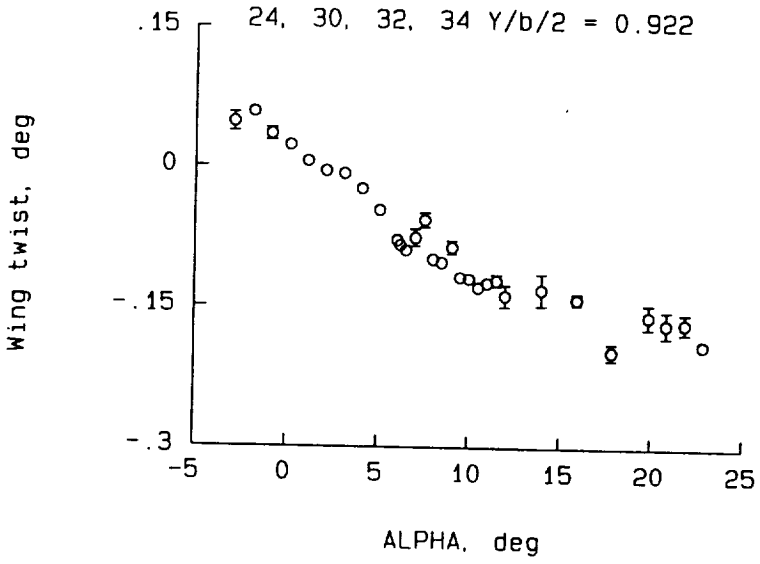

Figure 6. Mean wing twist corresponding to Table 2 for air runs at Mach = 0.3 and dynamic pressure = 153 psf. The standard deviations of the scatter are plotted as error bars if greater than the symbol size. Y/b/2 = 0.922.

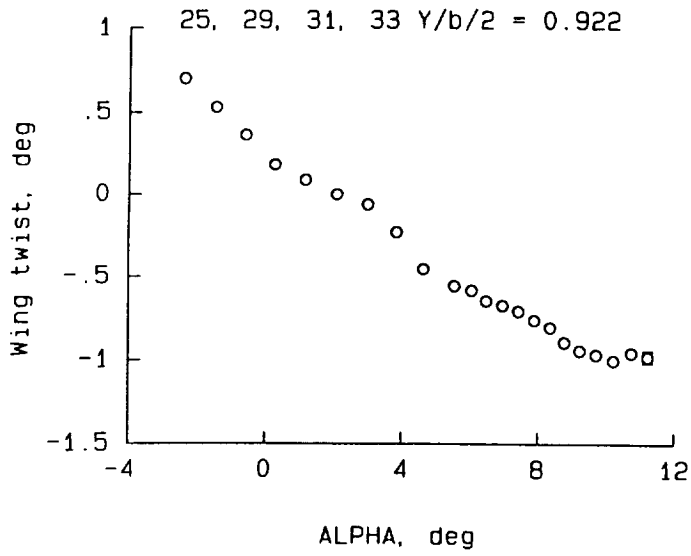

Figure 7. Mean wing twist corresponding to Table 2 for air runs at Mach = 0.9 and dynamic pressure = 965 psf. The standard deviations of the scatter are plotted as error bars if greater than the symbol size. Y/b/2 = 0.922.

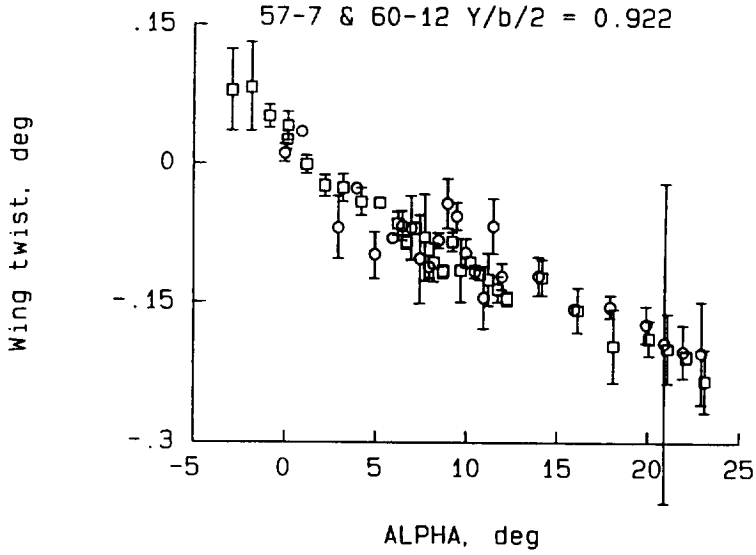

Figure 8. Wing twist corresponding to Table 6 for an air run at M = 0.3 and dynamic pressure = 154 psf. Y/b/2 = 0.922.

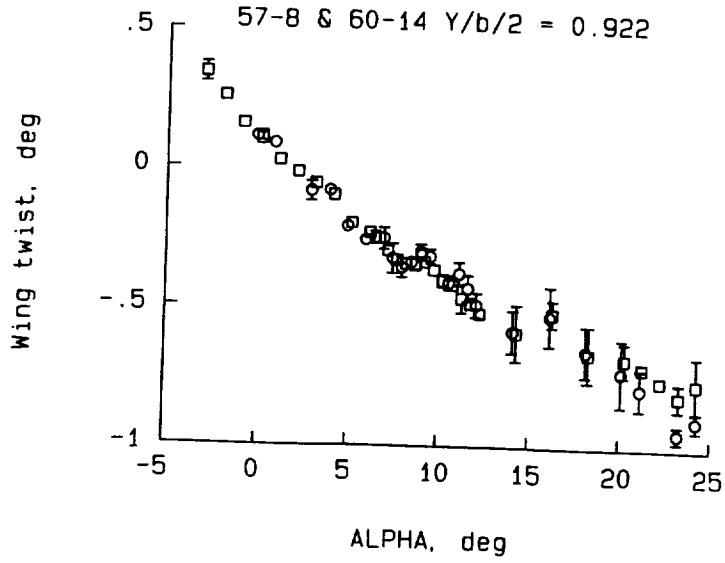

Figure 9. Wing twist corresponding to Table 6 for an air run at M = 0.6 and dynamic pressure = 534 psf. Y/b/2 = 0.922.

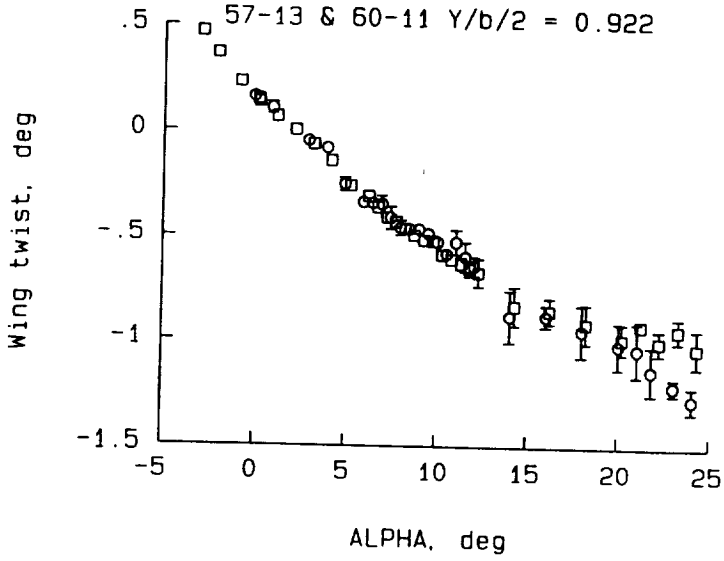

Figure 10. Wing twist corresponding to Table 6 for an air run at M = 0.3 and dynamic pressure = 804 psf. Y/b/2 = 0.922.

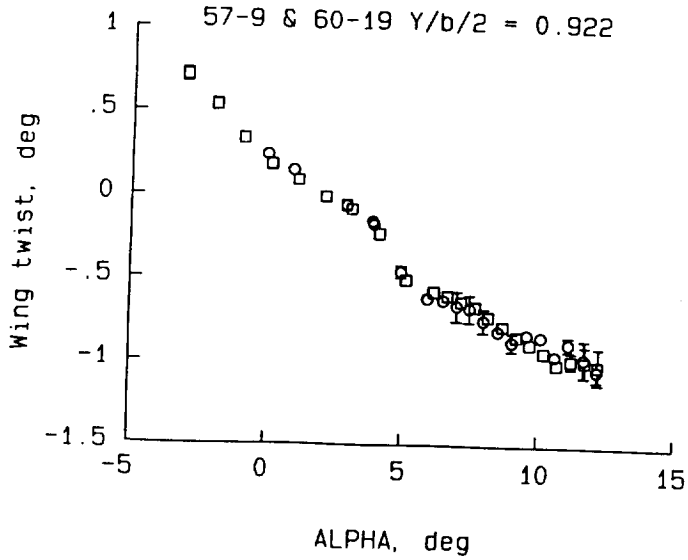

Figure 11. Wing twist corresponding to Table 6 for an air run at M = 0.9 and dynamic pressure = 967 psf. Y/b/2 = 0.922.

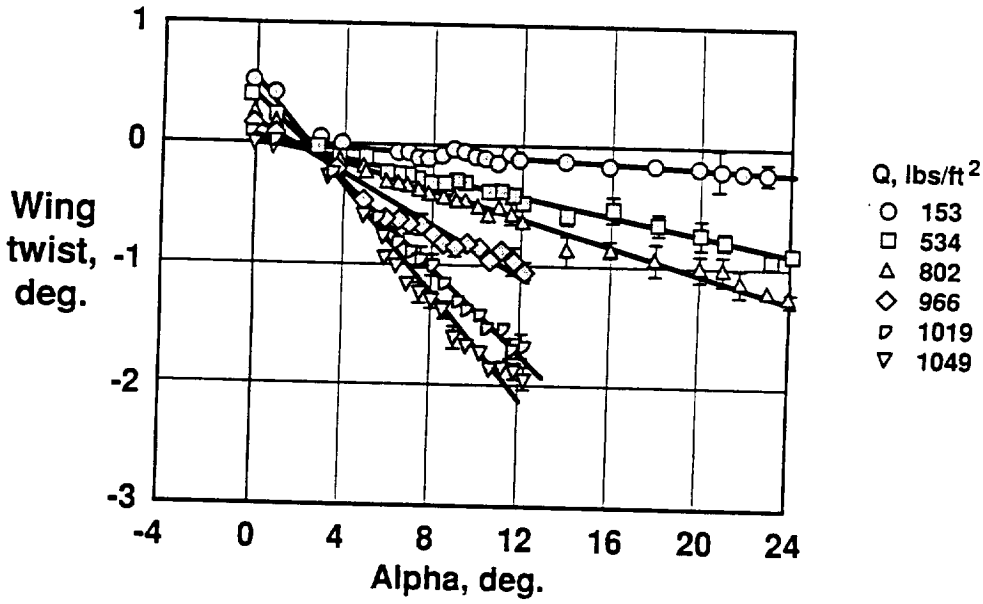

Figure 12. Wing twist for air runs at varying dynamic pressure. Y/b/2 = 0.922.

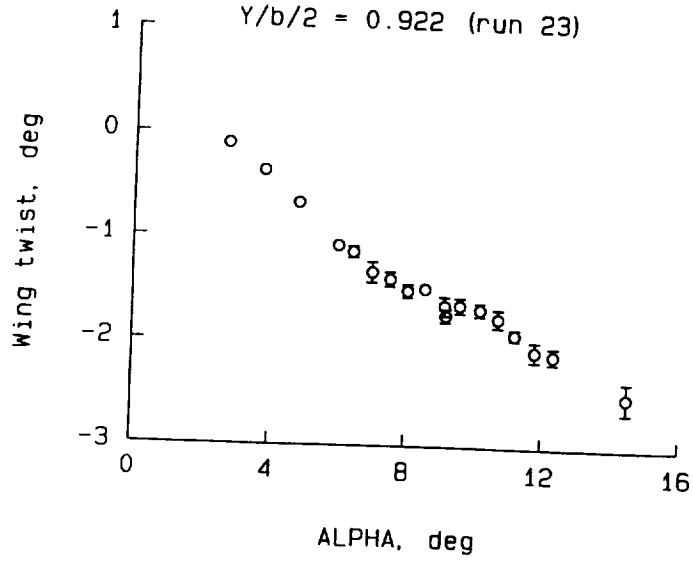

Figure 13. Wing twist for a nitrogen run at -152 F, Mach number of 0.6, and dynamic pressure of 2670 psf. Y/b/2 = 0.922.

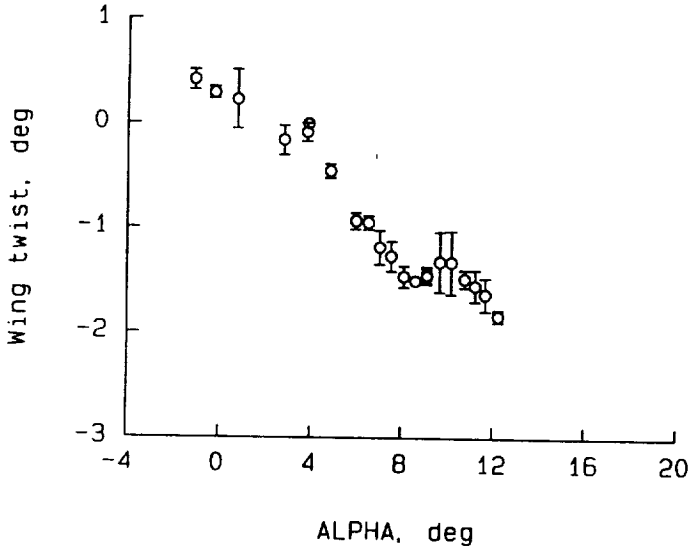

Figure 14. Wing twist for a nitrogen run at -250 F, Mach number of 0.9, and dynamic pressure = 1795 psf. Y/b/2 = 0.922.

REPORT DOCUMENTATION PAGE

Form Approved
OMB No. 0704-0188

1. AGENCY USE ONLY *(Leave blank)*	2. REPORT DATE	3. REPORT TYPE AND DATES COVERED
	February 1996	Technical Memorandum

4. TITLE AND SUBTITLE
Wing Twist Measurements at the National Transonic Facility

5. FUNDING NUMBERS
505-59-54-01

6. AUTHOR(S)
Alpheus W. Burner, Richard A. Wahls, and William K. Goad

7. PERFORMING ORGANIZATION NAME(S) AND ADDRESS(ES)
NASA Langley Research Center
Hampton, VA 23681-0001

8. PERFORMING ORGANIZATION REPORT NUMBER

9. SPONSORING / MONITORING AGENCY NAME(S) AND ADDRESS(ES)
National Aeronautics and Space Administration
Washgton, DC 20546-0001

10. SPONSORING / MONITORING AGENCY REPORT NUMBER
NASA TM 110229

11. SUPPLEMENTARY NOTES

12a. DISTRIBUTION / AVAILABILITY STATEMENT
Unclassified-Unlimited

Subject Category 35

12b. DISTRIBUTION CODE

13. ABSTRACT ***(Maximum 200 words)***

A technique for measuring wing twist currently in use at the National Transonic Facility is described. The technique is based upon a single camera photgrammetric determination of two dimensional coordinates with a fixed (and known) third dimensional coordinate. The wing twist is found from a conformal transformation between wind-on and wind-off 2-D coordinates in the plane of rotation. The advantages and limitations of the technique as well as the rationale for selection of this particular technique are discussed. Examples are presented to illustrate run-to-run and test-to-test repeatability of the technique in air mode. Examples of wing twist in cryogenic nitrogen mode are also presented.

14. SUBJECT TERMS
Model Deformation. Wind Tunnel; Wing Twist; Cryogenics; Photogrammetry; and Video

15. NUMBER OF PAGES
23

16. PRICE CODE
A03

17. SECURITY CLASSIFICATION OF REPORT	18. SECURITY CLASSIFICATION OF THIS PAGE	19. SECURITY CLASSIFICATION OF ABSTRACT	20. LIMITATION OF ABSTRACT
Unclassified	Unclassified		